Gust Loads Alleviation Using Sloshing Fuel

J.J. De Courcy[*], L. Constantin [†], B. Titurus [‡], T.C.S. Rendall [§] and J.E. Cooper [¶]
University of Bristol, Bristol, BS8 1TR, UK

There is much interest in developing concepts to reduce in-flight loads resulting from gusts and atmospheric turbulence, as this will lead to lighter aircraft with improved fuel performance and reduced environmental impact. Recent work has considered using sloshing in tanks as a means to increase the effective structural damping in the wings. Experimental studies have quantified the effect that sloshing can have on simple systems, and these studies have been complemented by the development of equivalent mechanical models to efficiently model the process and provide a design capability. This paper provides an initial study to evaluate the benefits of fuel tank sloshing on the response of a simple simulated aeroelastic wing model subjected to "one minus cosine" vertical gust sequences. The effects of the filling level and tank position upon loads alleviation are explored. It is shown that the sloshing fuel can increase the damping level in the gust response, but is dependent upon the tank filling level, and tank size and position.

I. Nomenclature

$\mathbf{A}$	=	Structural stiffness matrix
a_w	=	Lift curve slope
$\mathbf{B}$	=	Aerodynamic damping matrix
$\mathbf{C}$	=	Aerodynamic stiffness matrix
C_z	=	Barrier damping
c	=	Wing chord
$\mathbf{E}$	=	Structural inertia matrix
EI	=	Flexural rigidity
ec	=	Distance of aero centre to flexural axis
F	=	Force
g	=	Gravitational acceleration
GJ	=	Torsional rigidity
$\underline{h}$	=	Gust weighting vector
K_z	=	Barrier stiffness
L	=	Lift
L_g	=	Gust length
M	=	Pitching moment
M_f	=	Fuel mass
$M_{\dot{\theta}}$	=	Pitch damping derivative
m_w	=	Wing mass per unit area
$\underline{q}$	=	Generalised coordinates
q_i	=	i^{th} generalised coordinate
s	=	Wing semi span
T	=	Kinetic energy
U	=	Potential energy
V	=	Airspeed
δW	=	Incremental work done

---

[*]PhD Student, Department of Aerospace Engineering
[†]PhD Student, Department of Aerospace Engineering
[‡]Senior Lecturer, Department of Aerospace Engineering
[§]Senior Lecturer, Department of Aerospace Engineering
[¶]Sir George White Professor of Aerospace Engineering, Department of Aerospace Engineering, FAIAA.

x, y, z	=	Chordwise, spanwise, out of plane distance
x_f	=	Chordwise position of flexural axis
x_m	=	Chordwise position of mass axis zz
Z_f	=	Ball free travel distance
θ	=	Wing twist
ρ	=	Air density
$\hat{(\ )}$	=	Maximum value normalisation
$\dot{(\ )}$	=	Derivative with respect to time

II. Introduction

All aircraft are subjected to dynamic loads resulting from in-flight atmospheric gusts and turbulence, with the resulting stresses determining the sizing, and hence weight, of the resulting structure [1]. There is much interest in developing active [2] (using the control surfaces) and passive (including composite tailoring [3] and folding wing-tips [4]) approaches to alleviate these loads, leading to more fuel-efficient and environmentally friendly airplane designs. Recent work, as part of the H2020 SLOW-D project, is considering the use of fuel sloshing as a means of reducing the loads effect of gusts and turbulence via increased damping. This research has used a combined numerical modelling and experimental approach. In the civil engineering field, there have been many cases of using some form of fluid in a tank as a tuned mass damper to reduce the lateral response of tall buildings to the wind or earthquakes [5, 6]; however, the majority of investigations have considered sloshing in a lateral direction. Some works have considered damping in vertical vibratory systems with extensive work being carried out on particle impact damping, where energy is dissipated through momentum exchange between particles of different sizes and the structure [7]. Vertically excited systems containing liquids have also been studied previously, with applications such as liquid propellant tanks or water towers [8–10]. Relatively little work has considered the use of fuel sloshing for loads alleviation for aircraft structures, with preliminary studies focused on numerical investigations on integration of fuel sloshing in aeroelastic models [11]. Tuned mass dampers are often used in civil aircraft to reduce the vibration and noise associated with engines [12] or aeroelastic response [13], but they tend to consist of mechanical systems rather than sloshing of a fluid in a tank and have not been applied to gust or turbulence loads. There is a need to be able to develop validated mathematical models of the coupled wing / fuel-sloshing process to enable exploitation of the potential added damping benefits of the sloshing motions via novel wing / tank designs. In particular, the use of smoothed particle hydrodynamics (SPH) and equivalent mechanical model (EMM) methods in fluid sloshing and fluid-structure interaction research is well established [14] and these have been employed by the authors previously [15]. The use of EMM methodology in fluid sloshing problems has long history [8] and provides a much simpler and computational less expensive formulation of the dynamics of sloshing systems. An updated and comprehensive list of such approaches for modelling sloshing behaviour can be found in references [14, 15]. Previous experiments as part of the SLOW-D project have considered the overall transient acceleration response of a cantilever beam [16, 17] and a single DOF "T-beam" system [15] subjected to vertical sloshing motion. It was found that the presence of the fluid significantly increases the inherent damping in the system, but this is dependent upon the filling level of the tank and the size of motion. The maximum amount of damping was achieved at a 50% fill level, with the system showing three distinct damped response regimes during the transient decay related to different motions of the fluid. The T-beam study [15] concentrated upon the first response regime, immediately at the start of the transient, where the fluid motion is turbulent and involves significant impacts of the fluid on the tank floor and ceiling. The experimental tests were compared successfully with numerical simulations using SPH and EMM (based upon a bouncing ball) to model the fluid motion and both methods gave a reasonable representation of the experimental results, particularly for the initial damping zone.

A. Previous Experimental Tests

Recent experimental investigations into the effects of vertical sloshing have been performed using the T-beam SDOF rig [15] shown in Fig. 1 and the cantilevered beam configuration [16, 17] illustrated in Fig. 2. These studies investigated the effect of different levels of fluid fill, and also size of initial deflection, on the damping characteristics of the transient response. The addition of the fluid was found to dramatically increase the effective or overall damping level. Similar results were obtained in this study, as exemplified in Fig. 3, where two time series for the wing's motion are presented. The addition of the fluid model is seen to increase the energy dissipation in a similar fashion as observed in all the previous studies. Analysis of these responses for various systems [15–17] shows that they can be characterised by

a piece-wise linear damping behaviour observed on the logarithm of the decaying motion envelopes. It was found that the different zones correlate with particular flow regimes occurring at those time instants; one example of this is shown in Fig. 4, where the envelope of acceleration signals are presented on a semi-logarithmic scale. It can be seen that experiments and different numerical models demonstrate the existence of various damping regions with different damping ratios.
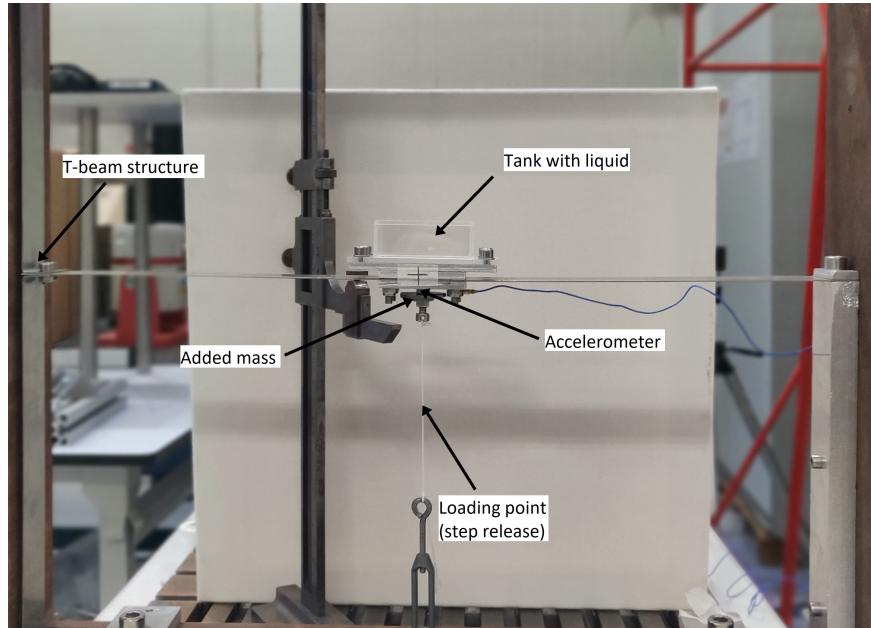

Fig. 1 SDOF T-Beam experiment [15].
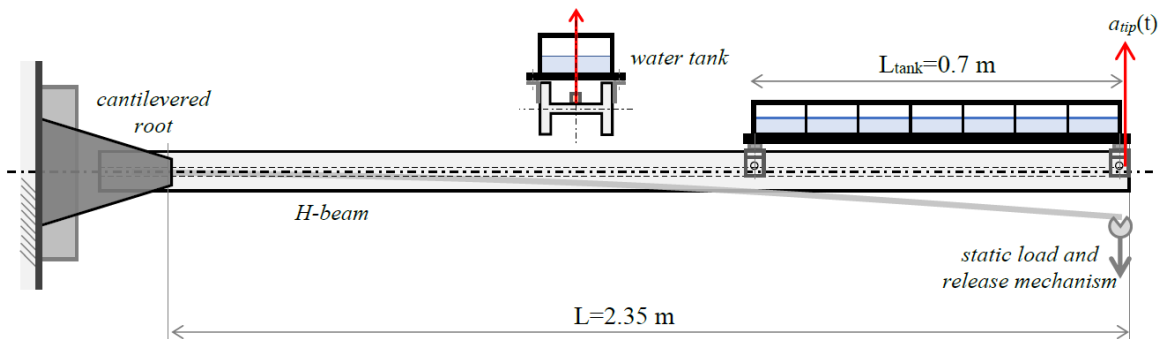
Fig. 2 Cantilever beam experiment with sloshing tanks [16].

B. Typical One DOF Sloshing Results

Figure 4 shows a typical comparison from previous vertical sloshing studies [15] between the two analysis methods and the experimental results for the SDOF system. It can be seen that there is a good correlation between the predicted acceleration envelopes for the initial region (R1 in Fig. 4). This region is the most important for gust alleviation as it corresponds to the largest response amplitudes and damping ratios and also it is usually the first one occurring immediately after excitation. The subsequent R2 regime represents decreased fluid-induced damping as liquid motion settles to vertically excited Faraday waves [18], before reaching R3 which converges to the dry structural damping conditions. Even though the damping ratio is lower in R2 when compared to R1, substantial amounts of energy were
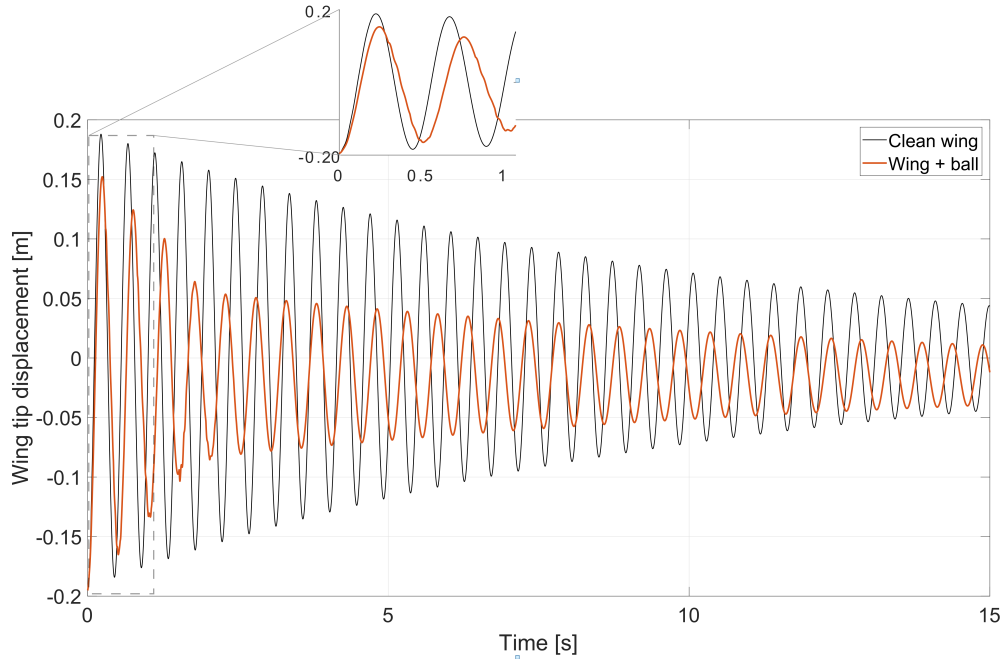
3

Fig. 3   Transient response of wing model, with and without bouncing ball

found to be dissipated by projecting the liquid's motion onto one of its sloshing modes.

This work builds upon the previous studies to investigate the potential benefits of fuel tank sloshing on the response of a simple simulated aeroelastic wing model subjected to "one minus cosine" vertical gust sequences. The effects of the filling level and tank position upon loads alleviation are explored for different gust lengths.
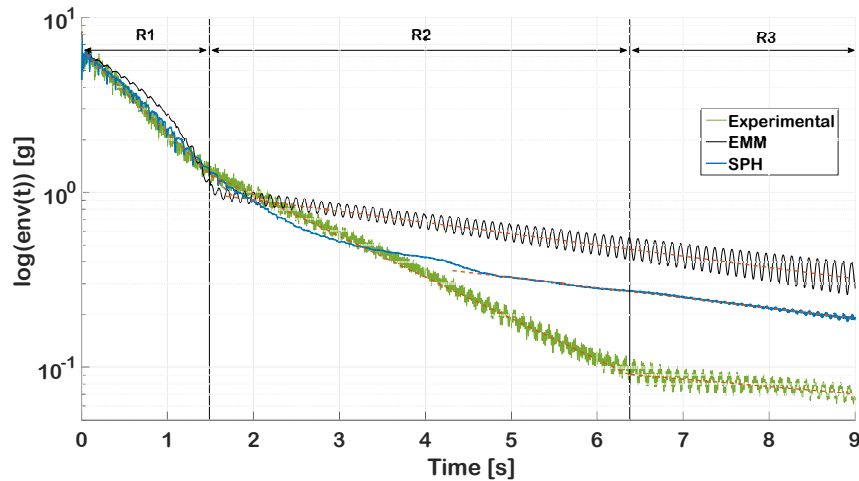

Fig. 4   Acceleration envelopes for the 50% filling level case; experimental vs SPH & EMM responses.

III. Aeroelastic Modelling

There are many ways that aeroelastic models of representative wings can be formulated [1]. Previous work focused upon aeroelastic tailoring [3, 19] has shown how simple modified unsteady strip theory aerodynamics coupled to beam models can produce surprising representative predictions of aeroelastic response and stability boundaries. In this initial

4

study a representative beam model is coupled to modified unsteady strip theory aerodynamics including a defined vertical gust sequence coupled, in turn, to an EMM sloshing model resulting in the simplified overall system set-up shown in figure 5.

The wing and aerodynamic models follow directly from [1] for an unswept, untapered wing with two out-of-plane bending and two torsion modes. Considering Fig. 6 and assuming a deflection shape of

$$z = y^2 q_1 + y^3 q_2 + y \left(x - x_f \right) q_3 + y^2 \left(x - x_f \right) q_4 \tag{1}$$

from which the twist is defined as

$$\theta = y q_3 + y^2 q_4 \tag{2}$$

then by applying a Lagrangian approach, see the appendix for the full derivation, the structural equations take the form

$$\mathbf{A}\ddot{\underline{q}} + \mathbf{E}\underline{q} = \underline{0} \tag{3}$$

The aerodynamic terms are added using a modified unsteady strip theory [1] defining the lift and pitching moment on each incremental strip respectively as

$$dL = \frac{1}{2}\rho V^2 c\, dy\, a_w \left(\frac{y^2 \dot{q}_1 + y^3 \dot{q}_2}{V} + y q_3 + y^2 q_4 + \frac{w_g}{V} \right) \tag{4}$$

$$dM = \frac{1}{2}\rho V^2 c^2 dy \left[e a_w \left(\frac{y^2 \dot{q}_1 + y^3 \dot{q}_2}{V} + y q_3 + y^2 q_4 + \frac{w_g}{V} \right) + M_{\dot\theta} c \frac{\left(y \dot{q}_3 + y^2 \dot{q}_4 \right)}{4 V} \right] \tag{5}$$

By considering the incremental work that is performed by the lift and moment on each incremental strip, the aerodynamic damping and aerodynamic stiffness matrices can be introduced into the aeroelastic equations, including a vertical gust field w_g, such that

$$\mathbf{A}\ddot{\underline{q}} + \rho V \mathbf{B}\dot{\underline{q}} + \left(\rho V^2 \mathbf{C} + \mathbf{E} \right) \underline{q} = \underline{h} w_g \tag{6}$$

Table 1   Parameters for the 4-modes aeroelastic model [1]

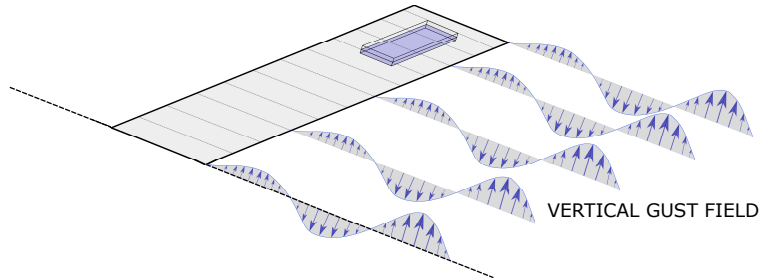| s	$7.5\ m$	c	$2\ m$
x_f	$0.48c$	x_m	$0.5c$
m_w	$200\ kg m^{-2}$	EI	$2e+7\ Nm^2$
GJ	$2e+6\ Nm^2$	a_w	2π
$M_{\dot\theta}$	-1.2	ρ	$1.225\ kg m^{-3}$

VERTICAL GUST FIELD

Fig. 5   Schematic of wing and tank encountering a vertical gust field.
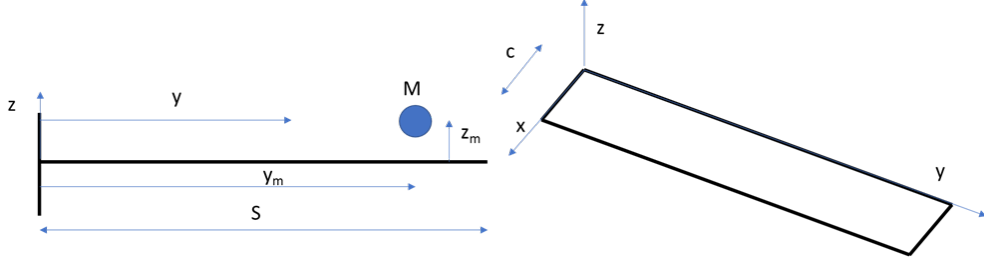
Fig. 6   Wing mathematical model.

IV. Sloshing EMM model

An equivalent mechanical model based upon a bouncing ball has been developed, aiming to model the fluid induced damping behaviour primarily from vertical excitation. Previous work focused upon a fixed-mass particle bouncing vertically within the T-beam tank, Fig.1, where collisions were modelled through an instantaneous inelastic impact. Mass and vertical travel distance of the particle were a function of tank geometry and filling level with respect to the true sloshing conditions. Dissipation was induced through a coefficient of restitution at impact, chosen according to an optimisation procedure tuning the EMM against experimentally evaluated damping ratios across multiple excitation and tank filling levels [15]. This simplified model provides an effective representation of the fluid induced damping during the violent sloshing regimes observed under high vertical accelerations, as shown in figure 4.

Within the current work, a comparable EMM is developed for coupling with the previously discussed wing model to assess the influence of fuel slosh on the aeroelastic response. To facilitate coupling of the models the coefficient of restitution condition, which implies instantaneous impact and spatially discrete momentum transfer, is replaced with a set of "barrier functions". These apply stiffness and damping forces in the vicinity of tank boundaries to approximate rigid impact conditions. Additionally, a continuous ball-to-wing coupling is maintained through spatially nonlinear barrier functions with free-play equivalent to the vertical travel range of the fluid particle, enabling continuous temporal integration without the need for impact detection. The developed EMM is subsequently detailed.

The position of the fluid particle is taken at the midpoint of the chosen tank domain, where the vertical wing deflection z_a is reconstructed according to the assumed mode shapes of Eqn.1. The fluid particle is assigned mass M_f equal to the considered fluid and moves freely in the vertical region $[-Z_f, Z_f] + z_a$ under gravity, where Z_f is the range of free travel set by tank height and fluid filling level. The absolute position of the ball z_m is constrained to the tank boundaries through the introduction of viscoelastic impact forces which act on both fluid and wing elements. The total barrier force F_{sb} is composed of two elements, the first an elastic and smooth barrier force [20] defined as

$$F_{sb}(r) = \frac{K_z}{\pi} \left[(r + Z_f) \left(\frac{\pi}{2} + \tan^{-1} \frac{-(r + Z_f)}{\epsilon_s} \right) + (r - Z_f) \left(\frac{\pi}{2} + \tan^{-1} \frac{(r - Z_f)}{\epsilon_s} \right) \right] \tag{7}$$

where $r = z_m - z_a$ is the relative position of the ball from the wing attachment point, K_z the asymptotic barrier stiffness and ϵ_s a factor influencing the function smoothness at the barrier $r = Z_f$. This function is shown graphically within Fig.7a where the inset shows the participation of ϵ_s on smoothing stiffness at the barrier. In addition to stiffness, a penetration damping [21] is employed to ensure fluid-induced dissipation is present within the system, defined as

$$F_{cb}(r, \dot{r}) = f_1(r) f_2(r, \dot{r}) C_z \dot{r} \tag{8}$$

where C_z is the viscous damping coefficient. The penetration damping control functions have the form

$$f_1(r) = h(r) - h(-r)$$

$$f_2(r, \dot{r}) = H(r)H(\dot{r}) + H(-r)H(-\dot{r})$$

where H is the Heaviside function, and h the auxiliary ramp-step function

$$h(r) = \left[H\left(r - Z_f\right) - H\left(r - (Z_f + \epsilon_D)\right) \right] \frac{r - Z_f}{\epsilon_D} + H\left(r - (Z_f + \epsilon_D)\right) \tag{9}$$

The combination of these functions ensures a smooth damping transitions upon penetrating the boundary, with magnitude dependent on relative velocity, as in Fig.7b. Coefficients K_z, ϵ_s and ϵ_d are chosen to give the required rigid impact

6

conditions whilst maintaining smooth enough functions to permit good numerical time integration. From the previously derived coefficient of restitution for a fluid [15] the equivalent wall damping ratio can be calculated from [22]. From the two viscoelastic forcing functions motion of the particle is simply defined as

$$M_f \ddot{z}_m = M_f g - F_{sb} - F_{cb} \tag{10}$$

Coupling is performed through the barrier forces F_{sb} and F_{cb} which act equal and opposite on both elements, the ball and wing at tank position. Barrier force is transformed into modal forcing through the linear transformation $\underline{F}_q = \underline{V}_a (F_{sb} + F_{cb})$, where $\underline{V}_a$ is the vector of modal participation factors at tank position (x_a, y_a). The complete coupled aeroelastic model thus takes the form

$$\begin{bmatrix} \mathbf{A} & 0 \\ \underline{0}^T & M_f \end{bmatrix} \begin{bmatrix} \ddot{\underline{q}} \\ \ddot{z}_m \end{bmatrix} + \begin{bmatrix} \rho V \mathbf{B} & 0 \\ \underline{0}^T & 0 \end{bmatrix} \begin{bmatrix} \dot{\underline{q}} \\ \dot{z}_m \end{bmatrix} + \begin{bmatrix} \rho V^2 \mathbf{C} + \mathbf{E} & 0 \\ \underline{0}^T & 0 \end{bmatrix} \begin{bmatrix} \underline{q} \\ z_m \end{bmatrix} = \begin{bmatrix} \underline{F}_q \\ M_f g - F_{sb} - F_{cb} \end{bmatrix} + \underline{h} w_g \tag{11}$$

which is transformed into state-space and integrated using Matlab's inbuilt time-stepping solvers.
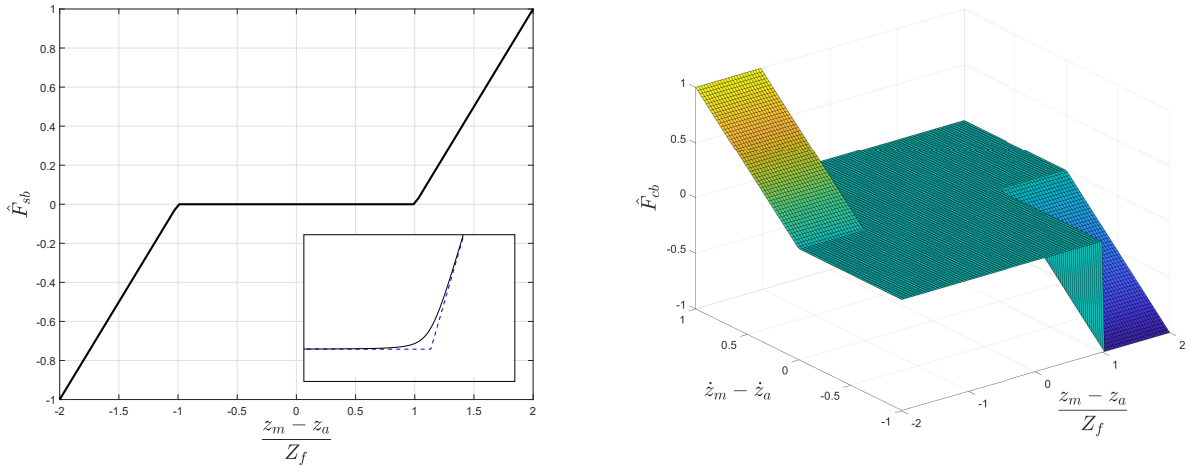
(a) Asymptotic stiffness coefficient, inset shows smoothed barrier condition.

(b) Damping coefficient versus ball position and velocity relative to tank.

Fig. 7   EMM viscoelastic barrier functions.

V. Results

A series of results are presented in this section showing the dissipation rate observed when the sloshing fluid is added to the aeroelastic wing model subjected to a vertical gust field.

Two models are considered here, i. the fully coupled system with ball motion and ii. a ball fixed to the wing representing the equivalent frozen mass case to ensure constant frequency and dynamic comparability. The ball position is chosen to represent the motion of fuel in outboard wing tanks which see larger acceleration compared to inboard fuel stores. It is assumed that at full tank filling the fuel has a mass of 10% of the wing. The tank depth is calculated from a representative aerofoil maximum thickness of 12%, leading to the particle free-flight range $Z_f = \frac{1}{2} 0.12c (1 - Fill)$, and a chordwise extent of 40% to represent torque box dimensions. A rectangular constant section wing is used to calculate the spanwise extent of the tank from the required fuel volume and density ($\rho_f = 810 kgm^{-3}$) and the ball placed at the midpoint of the tank inboard of the tip.

The total maximum energy inside a cycle was evaluated and the dissipation rate obtained by fitting an exponential curve over the region where the ball is bouncing inside the tank. This approach is demonstrated in Fig. 8 where the energy components, total energy and the exponential fit are shown against time for a representative gust input. The part of the transient that is relevant to this study is where the peak vertical acceleration at the tank position is greater than $1g$,

as $a > g$ is the condition for the ball to detach from the bottom of the tank. An exponential function is fitted over this part of the decaying motion and the decay constant is taken here as a measure of energy dissipation rate.

In order to gain insight into the behaviour of the coupled system, the study is divided into two parts: the wing with no aerodynamic interaction, $V = 0$, and imposed initial deflection, and the wing with aerodynamic forcing from the airflow $V \neq 0$ and the vertical gust field.

(a) Wing energy components.

(b) Exponential fit to wing energy across fluid response period.
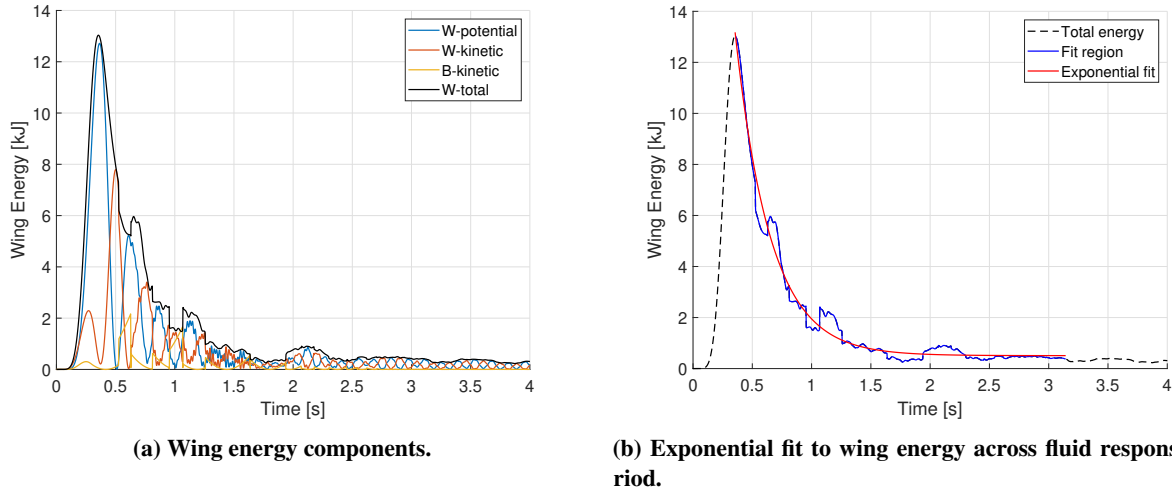
Fig. 8   Dissipation rate estimation from total wing energies during typical gust excitation.

A. Wind-off Case ($V = 0$)

In the case when the wing is not interacting with the air around it, the freestream velocity is set to 0 and consequently as there is no aerodynamic damping (or stiffness) a small amount of proportional structural damping was added. In this case the elastic axis is set to be coincident with the mass axis, so that there is no bending-torsion coupling. This is the simplest version of the analysed system and its purpose is to establish the effect of the bouncing ball on a simple cantilevered beam in the absence of any other damping effects and compare the observed behaviour with other results.

Fig. 3 clearly demonstrates the additional damping that the sloshing fluid imparts on the structural response, with figure 9 showing the variation of the energy dissipation rate with filling level for an initial tip deflection of $0.1c$. A step release transient simulation was run for each filling ratio and a second-degree polynomial was fitted through the data as there is a certain scatter. The dissipation rate can be seen to be maximized around the 50% fill level. Previous studies on 1dof systems have shown the same damping trend with filling level, with a maximum obtained at 50% fill as well [15]. The variation of dissipation rate with changing initial tip deflection for a constant filling ratio of 0.5 is presented in Fig. 10. An increase in dissipation rate can be observed up to a certain excitation level threshold. Similar behaviour was seen previously by the authors in simpler equivalent mechanical models, indicative of a damping saturation limit.

The response of the wing - bouncing ball coupled model shows behaviour consistent with previous findings considering 1DOF mass spring systems. In what follows, the aerodynamic model is added to the system along with a vertical gust field excitation.

B. Wind-on Case ($V \neq 0$)

Part of the airworthiness regulations considers the application of "one - cosine" (1MC) vertical gusts to the aircraft [1]. A range of different gust lengths are applied, whose maximum velocity is defined by the $H^{(1/6)}$ rule related to the flight altitude. The "discrete tuned gust" is the one that produces the largest response magnitude for which ever "interesting quantity" that is being considered. Here, the flight condition is taken as a velocity V of $70 \ m/s$ at sea level, and the wing tank position is varied in the chord-wise direction. The behaviour of the coupled system is studied under various filling levels, tank positions and gust lengths.

A series of single parameter sweeps are presented in Fig. 11. The energy dissipation rate variation is presented as a function of fill level (Fig. 11a) and gust length (Fig. 11b). The "wet" case here is represented by the fully coupled
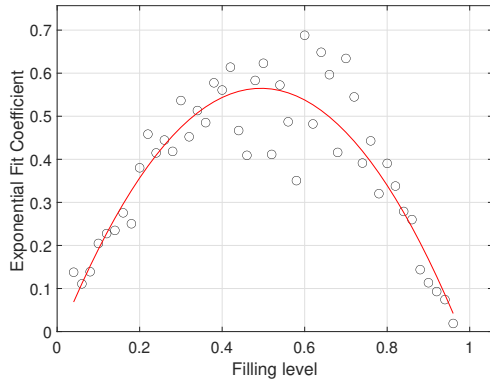
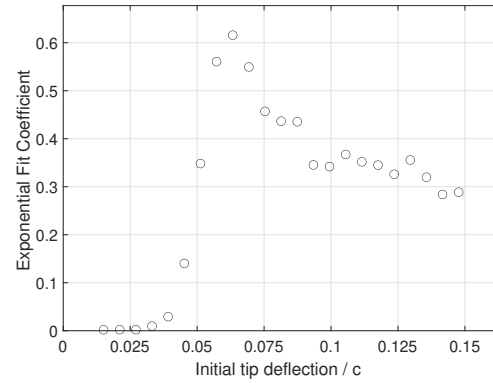**Fig. 9 Energy dissipation rate vs. filling level**

Fig. 10 Energy dissipation rate vs. initial deflection

system with the ball bouncing inside the tank, whilst the "dry" case is the baseline one represented by the wing with a point mass attached at the tank's position. The effect of the ball for these two cases is seen to be beneficial at lower filling levels and smaller gust lengths. This finding is somewhat different than what was obtained for the $V = 0$ case, where the dissipation rate was found to be maximized around the 50% filling level and to generally increase with excitation level up to a certain threshold. As we are considering a more complicated system than a single DOF, with coupling between torsion and bending motions and interactions with the airflow, we obtain more complex phenomena that influence the coupled behaviour between the ball and the wing model. A better image of the dissipation rate is obtained in 2-dimensional parametric maps, as shown in Figs. 12 and 14 where the ratio between the wet and dry dissipation coefficients is presented as function of gust length, fuel chordwise position and filling level.

Figure 12 shows the variation of energy dissipation coefficient of the wet (bouncing) case relative to the dry (fixed mass case), as a function of gust length L_g/c and tank chordwise position x/c. This dissipation map shows positive contributions by the introduction of the fuel model in blue and negative ones in red. In other words, more energy is dissipated when the ball is added to the system in the blue regions and the ball worsens the dissipation rate in the red regions. The gust lengths considered are limited to $32c$ as past that value the peak acceleration at the tank point does not exceed $1g$ and the ball does not get detached from the bottom of the tank.

Two main regions can be observed in Fig. 12: one of high sloshing-induced dissipation rates at low gust lengths (up to $L_g/c = 15$), and one of negative sloshing-induced dissipation rates at $L_g/c > 17$. For low gust lengths, as the position of the bouncing ball moves towards the leading edge (low values of x/c) the observed dissipation rate increases by up to 1.6 times the dry case value. The difference between the two damping behaviours with varying gust length can be understood by looking at the interaction between the bouncing ball and the torsional modes of the wing. Figure 13 shows a time history of wing tip angle of attack for points A and B in Fig. 12, for both wet and dry cases. While at point A, where the fuel model contributes positively to the energy dissipation rate, the angle of attack is reduced for the wet case, the reverse situation happens at point B: the bouncing ball adds energy in the torsional modes of the system as compared to the dry case. As the only parameter that was changed between the two points is the gust length, it follows that these results suggest that the beneficial interaction between the fuel and the wing may be restricted to certain gust lengths when particular modes are excited.

Figure 14 shows the energy dissipation rate map for the gust length and filling level parameters. Once again there are a range of responses depending upon the parameters. A positive contribution is seen in the wet case for the mid-range to high filling levels and lower gust lengths, whereas the high filling levels give a negative contribution for all gust lengths apart from the smallest.

9
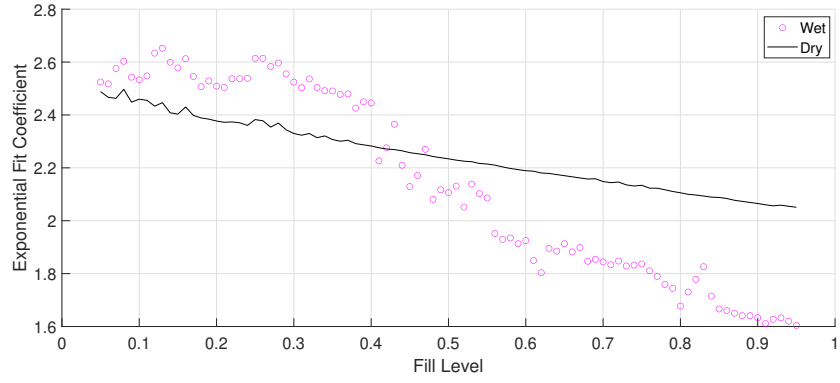
(a) Variation with tank filling level at fixed $19c$ gust length.
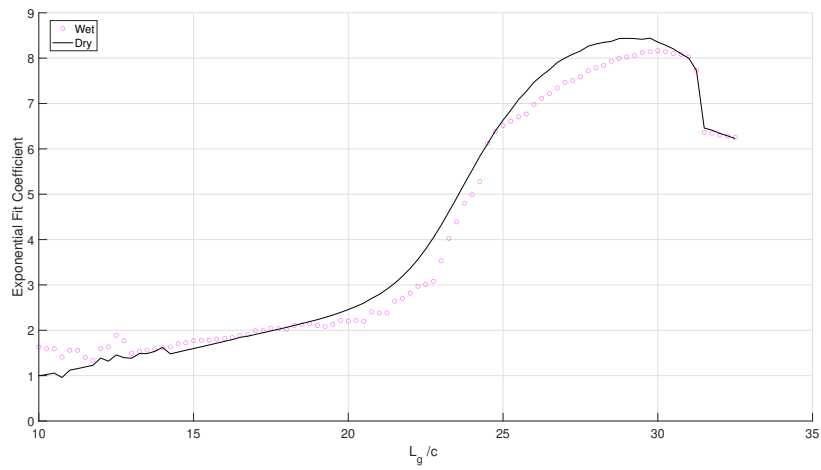
(b) Variation with gust length at 50% tank filling level.

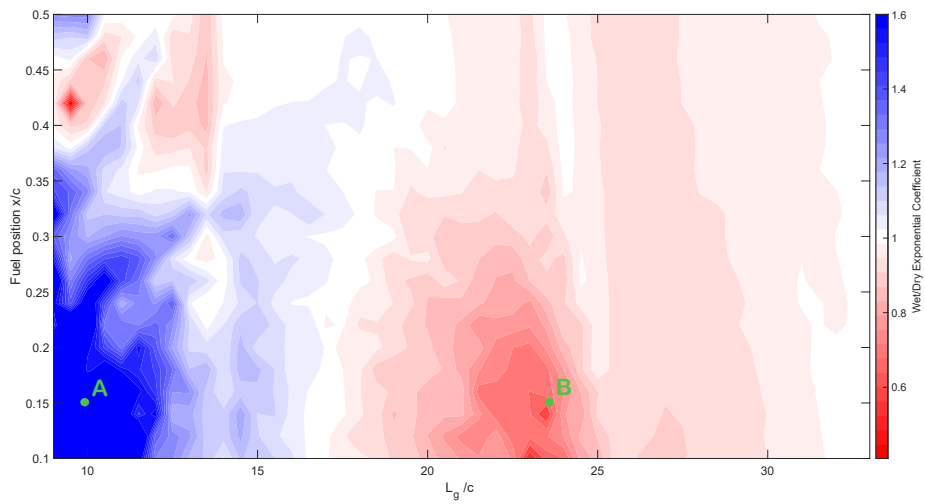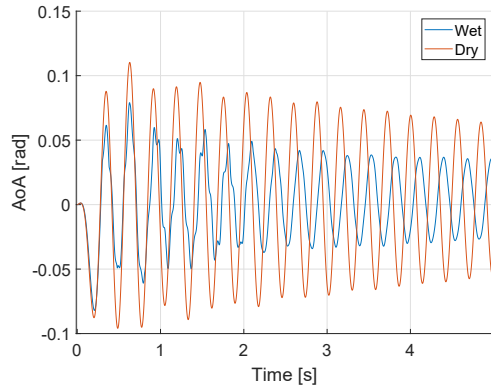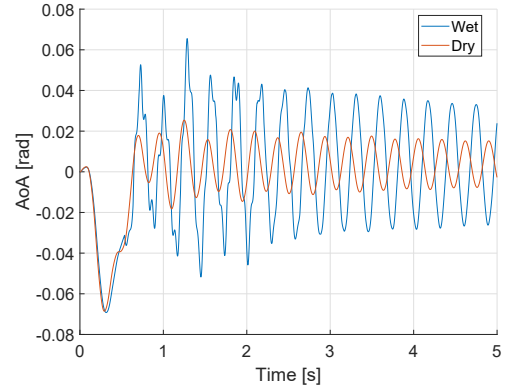**Fig. 11   Single parameter sweeps**

Fig. 12   Map of wet to dry damping coefficient versus gust length and chordwise fuel position. 50 % fill.

(a) Point A AoA in Fig. 12, $L_g/c = 10$, $x/c = 0.15$, **wet vs dry**

(b) Point B AoA in Fig. 12, $L_g/c = 23.5$, $x/c = 0.15$, **wet vs dry**

Fig. 13   Angle of attack variation with time for two points $(L_g, x/c)$ **in figure 12: A** $(10, 0.15)$ **and B** $(23.5, 0.15)$
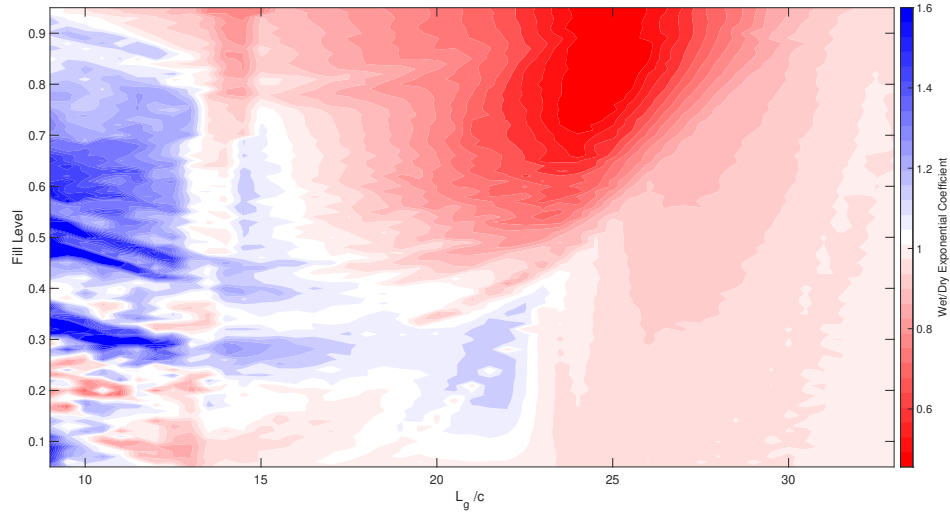

Fig. 14   Ratio of wet to dry damping coefficient versus filling level and gust length, tank positioned at quarter chord.

VI. Conclusions

Initial studies have been performed considering the effect of vertical sloshing motion in a fuel tank on the response of a representative aircraft wing subjected to 1-cosine vertical gust excitation. Unsteady strip theory applied to a beam model provided a baseline aeroelastic method for inclusion of sloshing physics. An equivalent mechanical model was developed to represent the motion of fuel and induced damping behaviour seen in vertically excited fluids. The fuel was modelled as a fixed mass particle moving in the vertical DOF, with nonlinear stiffness and damping barier behaviour to represent the particle free flight and fluid impacting conditions. The system was considered for varying fuel fill, tank chordwise position and different "one-minus-cosine" gust lengths. Categorising the damping effect is more complicated than previous studies considering single DOF mechanical systems with no aerodynamic coupling. The damping effect from sloshing was generally positive compared to the dry case for shorter gust lengths with the maximum damping occurring at around 50 % fill. However, beyond moderate to longer gust lengths the effect of the sloshing fluid was often detrimental to the transient response. Further work is required to study the effects of sloshing fluids in wing tanks in more detail.

Acknowledgments

Appendix

Considering an unswept, untapered wing with two out-of-plane bending and two torsion modes and constant mass distribution [1], as shown in figure 6. A assuming a deflection shape of

$$z = y^2 q_1 + y^3 q_2 + y \left(x - x_f \right) q_3 + y^2 \left(x - x_f \right) q_4 \tag{A.1}$$

from which the twist is defined as

$$\theta = y q_3 + y^2 q_4 \tag{A.2}$$

Applying a Lagrangian approach, the total kinetic and elastic potential energies can be shown to be

$$T = \frac{m}{2} \int_0^s \int_0^c \left(y^2 \dot{q}_1 + y^3 \dot{q}_2 + y \left(x - x_f \right) \dot{q}_3 + y^2 \left(x - x_f \right) \dot{q}_4 \right)^2 \, dx dy \tag{A.3}$$

and

$$U = \frac{1}{2} \int_0^s EI \left(2q_1 + 6y q_2 \right)^2 dy + \frac{1}{2} \int_0^s GJ \left(q_3 + 2y q_4 \right)^2 dy \tag{A.4}$$

Application of Lagrange's equation for each of the generalised coordinates leads to the structural matrix equations,

$$
\begin{bmatrix}
\frac{s^5 c}{5} & \frac{s^6 c}{6} & \frac{s^4}{4}\left(\frac{c^2}{2} - c x_f\right) & \frac{s^5}{5}\left(\frac{c^2}{2} - c x_f\right) \\
\frac{s^6 c}{6} & \frac{s^7 c}{7} & \frac{s^5 c}{5}\left(\frac{c^2}{2} - c x_f\right) & \frac{s^6 c}{6}\left(\frac{c^2}{2} - c x_f\right) \\
\frac{s^4}{4}\left(\frac{c^2}{2} - c x_f\right) & \frac{s^5}{5}\left(\frac{c^2}{2} - c x_f\right) & \frac{s^3}{3}\left(\frac{c^3}{3} - c 2 x_f + c x_f^2\right) & \frac{s^4}{4}\left(\frac{c^3}{3} - c 2 x_f + c x_f^2\right) \\
\frac{s^5}{5}\left(\frac{c^2}{2} - c x_f\right) & \frac{s^6}{6}\left(\frac{c^2}{2} - c x_f\right) & \frac{s^4}{4}\left(\frac{c^3}{3} - c 2 x_f + c x_f^2\right) & \frac{s^5}{5}\left(\frac{c^3}{3} - c 2 x_f + c x_f^2\right)
\end{bmatrix}
\begin{bmatrix} \ddot{q}_1 \\ \ddot{q}_2 \\ \ddot{q}_3 \\ \ddot{q}_4 \end{bmatrix}
$$
$$
+
\begin{bmatrix}
4\,\text{EI}s & 6\,s^2 EI & 0 & 0 \\
6\,s^2 EI & 12\,s^3 EI & 0 & 0 \\
0 & 0 & GJ_S & GJs^2 \\
0 & 0 & GJs^2 & \frac{4}{3}GJs^3
\end{bmatrix}
\begin{bmatrix} q_1 \\ q_2 \\ q_3 \\ q_4 \end{bmatrix}
=
\begin{bmatrix} 0 \\ 0 \\ 0 \\ 0 \end{bmatrix}
\tag{A.5}
$$

The aerodynamic terms are added using a modified unsteady strip theory, lift and pitching moment on a spanwise strip are defined as

$$dL = \frac{1}{2}\rho V^2 c \, dy \, a_w \left(\frac{y^2 \dot{q}_1 + y^3 \dot{q}_2}{V} + y q_3 + y^2 q_4 + \frac{w_g}{V} \right) \tag{A.6}$$

12

$$dM = \frac{1}{2}\rho V^2 c^2 dy \left[ea_w \left(\frac{y^2\dot{q}_1 + y^3\dot{q}_2}{V} + yq_3 + y^2 q_4 + \frac{w_g}{V} \right) + M_{\dot{\theta}} c \frac{(y\dot{q}_3 + y^2\dot{q}_4)}{4 V} \right] \tag{A.7}$$

Considering the incremental work that is performed by the lift and moment on the incremental strip

$$\delta W = \int_{wing} \left[dL \left(-y^2\delta q_1 - y^3\delta q_2 \right) + dM \left(y\delta q_3 + y^2\delta q_4 \right) \right] \tag{A.8}$$

and then integrating over the semi-span, the aerodynamic damping and stiffness matrices are found to be

$$\rho V \begin{bmatrix} -\frac{ca_w s^5}{10} & -\frac{ca_w s^6}{12} & 0 & 0 \\ -\frac{ca_w s^6}{12} & -\frac{ca_w s^7}{14} & 0 & 0 \\ \frac{c^2 ea_w s^4}{8} & \frac{c^2 ea_w s^5}{10} & \frac{c^3 M_{\dot{\theta}} s^3}{24} & \frac{c^3 M_{\dot{\theta}} s^4}{32} \\ \frac{c^2 ea_w s^5}{10} & \frac{c^2 ea_w s^6}{12} & \frac{c^3 M_{\dot{\theta}} s^4}{32} & \frac{c^3 M_{\dot{\theta}} s^5}{40} \end{bmatrix} \begin{bmatrix} \dot{q}_1 \\ \dot{q}_2 \\ \dot{q}_3 \\ \dot{q}_4 \end{bmatrix} \tag{A.9}$$

$$\rho V^2 \begin{bmatrix} 0 & 0 & -\frac{ca_w s^4}{8} & -\frac{ca_w s^5}{10} \\ 0 & 0 & -\frac{ca_w s^5}{10} & -\frac{ca_w s^6}{12} \\ 0 & 0 & \frac{c^2 ea_w s^3}{6} & \frac{c^2 ea_w s^4}{8} \\ 0 & 0 & \frac{c^2 ea_w s^4}{8} & \frac{c^2 ea_w s^5}{10} \end{bmatrix} \begin{bmatrix} q_1 \\ q_2 \\ q_3 \\ q_4 \end{bmatrix} \tag{A.10}$$

Including a vertical gust field w_g, the full aeroelastic equations of motion take the form

$$A\underline{\ddot{q}} + \rho V B\underline{\dot{q}} + \left(\rho V^2 C + E \right) \underline{q} = \underline{h} w_g \tag{A.11}$$

where the gust vector $\underline{h}$ is found as

$$\underline{h} = \rho V c a_w \begin{bmatrix} -s^3/6 \\ -s^4/8 \\ ces^2/4 \\ ces^3/6 \end{bmatrix} \tag{A.12}$$

References

[1] Wright, J., and Cooper, J., *Introduction to Aircraft Aeroelasticity and Loads*, Aerospace Series, Wiley, 2014.

[2] Xu, J., and Kroo, I., "Aircraft design with active load alleviation and natural laminar flow," *Journal of Aircraft*, Vol. 51, No. 5, 2014, pp. 1532–1545.

[3] Stodieck, O., Cooper, J., Weaver, P., and Kealy, P., "Aeroelastic tailoring of a representative wing box using tow-steered composites," *AIAA journal*, 2017, pp. 1425–1439.

[4] Castrichini, A., Siddaramaiah, V. H., Calderon, D., Cooper, J., Wilson, T., and Lemmens, Y., "Preliminary investigation of use of flexible folding wing tips for static and dynamic load alleviation," *The Aeronautical Journal*, Vol. 121, No. 1235, 2017, pp. 73–94.

[5] Bouscasse, B., Colagrossi, A., Souto-Iglesias, A., and Cercos-Pita, J., "Mechanical energy dissipation induced by sloshing and wave breaking in a fully coupled angular motion system. I. Theoretical formulation and numerical investigation," *Physics of Fluids*, Vol. 26, No. 3, 2014, p. 033103.

[6] Bouscasse, B., Colagrossi, A., Souto-Iglesias, A., and Cercos-Pita, J., "Mechanical energy dissipation induced by sloshing and wave breaking in a fully coupled angular motion system. II. Experimental investigation," *Physics of Fluids*, Vol. 26, No. 3, 2014, p. 033104.

[7] Friend, R. D., and Kinra, V., "Particle impact damping," *Journal of Sound and Vibration*, Vol. 233, No. 1, 2000, pp. 93–118.

[8] Abramson, H. N., "The dynamic behavior of liquids in moving containers, with applications to space vehicle technology," 1966.

[9] Ibrahim, R., and Soundararajan, A., "Non-linear parametric liquid sloshing under wide band random excitation," *Journal of Sound and Vibration*, Vol. 91, No. 1, 1983, pp. 119–134.

[10] Ibrahim, R., and Heinrich, R., "Experimental investigation of liquid sloshing under parametric random excitation," 1988.

[11] Hall, J., Rendall, T., Allen, C., and Peel, H., "A multi-physics computational model of fuel sloshing effects on aeroelastic behaviour," *Journal of Fluids and Structures*, Vol. 56, 2015, pp. 11–32.

[12] "US Patent US4724923A, Vibration absorber with controllable resonance frequency," , 1986.

[13] "US Patent US20130092489A1, Aeroelastic tuned mass damper," , 2011.

[14] Ibrahim, R. A., *Liquid Sloshing Dynamics: Theory and Applications*, Cambridge University Press, 2005. https://doi.org/10. 1017/CBO9780511536656.

[15] Constantin, L., De Courcy, J., Titurus, B., Rendall, T., and Cooper, J. E., "Analysis of Damping From Vertical Sloshing in a SDOF System," , 2020. Article in Press, Available Online – Mechanical Systems and Signal Processing Journal.

[16] Gambioli, F., Usach, R. A., Kirby, J., Wilson, T., and Behruzi, P., "Experimental Evalutation of Fuel Sloshing Effects on Wing Dynamics," *International Forum on Aeroelasticity and Structural Dynamics. Savannah, Georgia, USA, paper*, Vol. 139, 2019.

[17] Titurus, B., Cooper, J. E., Saltari, F., Mastroddi, F., and Gambioli, F., "Analysis of a Sloshing Beam Experiment," *International Forum on Aeroelasticity and Structural Dynamics. Savannah, Georgia, USA, paper*, Vol. 139, 2019.

[18] Ibrahim, R. A., "Recent advances in physics of fluid parametric sloshing and related problems," *Journal of Fluids Engineering*, Vol. 137, No. 9, 2015.

[19] Scarth, C., Sartor, P. N., Cooper, J. E., Weaver, P. M., and Silva, G. H., "Robust and reliability-based aeroelastic design of composite plate wings," *AIAA Journal*, 2017, pp. 3539–3552.

[20] Howcroft, C., Lowenberg, M., Neild, S., Krauskopf, B., and Coetzee, E., "Shimmy of an aircraft main landing gear with geometric coupling and mechanical freeplay," *Journal of Computational and Nonlinear Dynamics*, Vol. 10, No. 5, 2015.

[21] Yue, S., Titurus, B., Nie, H., and Zhang, M., "Liquid spring damper for vertical landing Reusable Launch Vehicle under impact conditions," *Mechanical Systems and Signal Processing*, Vol. 121, 2019, pp. 579–599.

[22] Nagurka, M., and Huang, S., "A mass-spring-damper model of a bouncing ball," *Proceedings of the 2004 American control conference*, Vol. 1, IEEE, 2004, pp. 499–504.